Basic Study on Wheel Speed Based Driving Force Control for Multi-motor Electric Vehicles with Glocal Stability Analysis

[1]Binh-Minh Nguyen, [1]Takumi Ueno, [1]Yuki Hosomi, [1]Tona Sato, [2]Shinji Hara, [1]Hiroshi Fujimoto
[1]The University of Tokyo, [2]Tokyo Institute of Technology
Email address of the corresponding author: nguyen.binhminh@edu.k.u-tokyo.ac.jp

***Abstract* – This paper presents a novel driving force control (DFC) strategy for electric vehicles driven by multi-motors. The proposed system is designed hierarchically, with driving force control in the outer-layer, and wheel speed control in the inner-layer. Notably, the outer-layer controller directly outputs the wheel speed references. This configuration does not requires the vehicle speed to calculate the wheel speed as the traditional DFC, thereby reducing system complexity. Moreover, this paper shows that the proposed system can be modelled as a multi-agent system with generalized frequency variable and a physical interaction matrix of rank-1. This allows us to guarantee the stability of the total system (global) with respect to the actuator dynamics (local). In particular, this paper establishes a D-stability condition, which is independent of the number of motor actuators. The proposed strategy is applied to range extension control via energy optimization by driving force distribution and control.**

Keywords – driving force, electric vehicle, in-wheel-motor, generalized frequency variable, range extension control.

I. INTRODUCTION

Thanks to the merits of motor actuator, motion control of electric vehicles (EVs) driven by multi-motor (Fig. 1) has been an active research field for years [1]. Typical examples are direct yaw moment control [2]-[3], energy optimization control [4]-[5], and vibration suppression [4]. This paper focuses on driving force control (DFC) [6]-[10], which has been shown an advanced traction method to generate the friction force between the tire and the road surface. The classical DFC is system is hierarchical, including the outer-layer force control and inner-layer wheel speed force. The DFC can effectively collaborate with the higher motion control layers, such as yaw-rate control [11]. To continuously develop and extend the applications of DFC, the following two issues need to be concerned.

The first issue is from an application point of view. In the classical DFC, the outer-layer is to generate the slip ratio reference signal y^*. Therefore, the vehicle speed is required to calculate from y^* the wheel speed reference. However, the vehicle speed sensor is of high cost, and it is not affordable for the commercial vehicles. The implementation of speed estimation algorithm will increase the complexity of the system design and analysis. In addition, any error in vehicle speed estimation will degrade the DFC performance.

The second issue is from a theoretical point of view. We consider an N-wheel-EV. Each wheel is provided with a local DFC. As discussed in [1] and [12], the multi-motor EV must be considered as multi-agent system, in which each controlled wheel is a local agent. The local agents interact with each other through the vehicle body. Thus, it is essential to guarantee the stability of the total system (global) with respect to the actuator dynamics (local). However, the glocal (global/local) stability analysis has not yet been developed for DFC of multi-motor EVs.

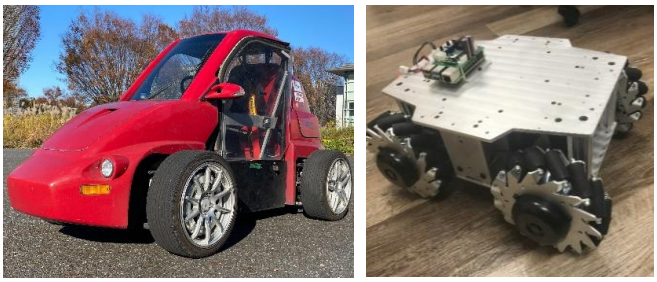

(a) 4 in-wheel-motor vehicle FPEV-2. (b) 4-mecanum-wheel-vehicle.

Fig. 1. Multi-motor vehicles at our research group.

With respect to the above issues, this paper is to present a novel strategy to DFC for multi-motor EVs. The strategy consists of a new control configuration, and a theoretical background to system analysis. Unlike the traditional DFC, the outer-layer force controller directly give the wheel speed reference. Furthermore, this paper shows that although the total system is quite complex, it can be represented as a multi-agent system using generalized frequency variable (GFV) [13]. Thanks to the GFV and the rank-1 matrix that representing physical interaction between the agents, the complexity of stability analysis is always the same, no matter what the number of motors installed to the vehicle body. In particular, this paper derives the **D**-stability condition for the proposed DFC.

This paper is to extend our recent study on wheel speed based DFC [10]. In this previous work, by using Circle criterion, the absolute stability analysis with respect to the wheel speed limiter was proposed. However, system design and evaluation were only performed using a single wheel model. Modeling and analyzing the DFC system for multi-motor EVs is still an open question.

The rest of this paper is organized as follows. Section II describes the vehicle dynamics. Section III presents the proposed DFC system. The glocal stability analysis and $\mathcal{D}$-stability condition are established in Section IV. Application of the proposed system to range extension control is presented in Section V. Finally, the conclusion is stated in Section VI.

II. MODELING

This paper examines the longitudinal motion of the EV driven by in-wheel-motor (IWM), as illustrated in Fig. 2. We let m be the vehicle mass; and v_x be the longitudinal speed of the vehicle. The rotational speed of the wheel is ω_i. Assuming that the wheels are physically homogeneous, we let J_w and r be the moment of inertia and the radius of all wheels, respectively. T_i, F_i, and Z_i represent the motor torque, the driving force, and the vertical force acting at the wheel, respectively. F_ξ is the disturbance force exerted on the vehicle body. As depicted in Fig. 2(b), the motion of a wheel is:

$$J_w\left(d\omega_i / dt\right) = T_i - rF_i \tag{1}$$

Let ε be a small positive number to avoid division-by-zero, the slip ratio λ_i is defined as

$$\lambda_i = \frac{\omega_i r - v_x}{\max\left\{\omega_i r, v_x, \varepsilon\right\}} \tag{2}$$

The driving force F_i can be expressed as

$$F_i = f_i(\lambda_i) \tag{3}$$

where $f_i(\,)$ is commonly described by the magic formula [14]. Besides, the longitudinal motion of the vehicle body is:

$$m\left(dv_x / dt\right) = \left(\sum_{i=1}^{N} F_i\right) - F_\xi = \mathbf{1}_N^{\mathrm{T}}\mathbf{F} - F_\xi \tag{4}$$

where F_ξ represents the disturbance (air resistance, road slope); $\mathbf{1}_N$ is the all-one-column vector of size N; and $\mathbf{F}$ is the vector which includes all local driving forces.

III. PROPOSED DRIVING FORCE CONTROL SYSTEM

This paper investigates the system in Fig. 3 where the EV plant includes N subsystem $\{\mathbf{W}_i\}$ interconnected via $\mathbf{V}$ - the vehicle body dynamics model. $\mathbf{T}$ and $\boldsymbol{\omega}$ are the vectors of size N which include the motor torques and the local speeds of the wheels. I_N represents the identity matrix of size N. F_{all} is the total driving force command which can be given by the driver, or the higher control layer. From (1), the driving force observer (DFO) is established as

$$\hat{F}_i = Q(s)\cdot\left(\frac{1}{r}T_i - \frac{J_w}{r}\cdot s\cdot\omega_i\right) \tag{5}$$

where the transfer function of the low-pass filter is

$$Q(s) = \frac{1}{\tau s + 1} \tag{6}$$

Each wheel is provided with a force controller $C_f(s)$ and a wheel speed controller $C_w(s)$. A Force Distribution Law (FDL) is to distribute F_{all}^* to the driving force reference vector $\mathbf{F}^*$.

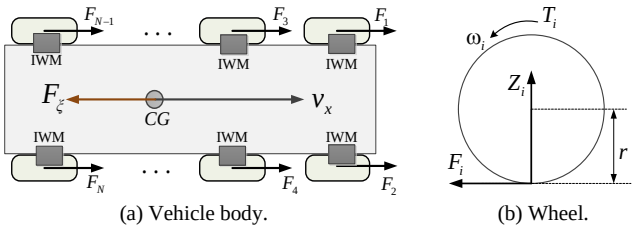

(a) Vehicle body. (b) Wheel.

Fig. 2. N-wheel-EV model under study.

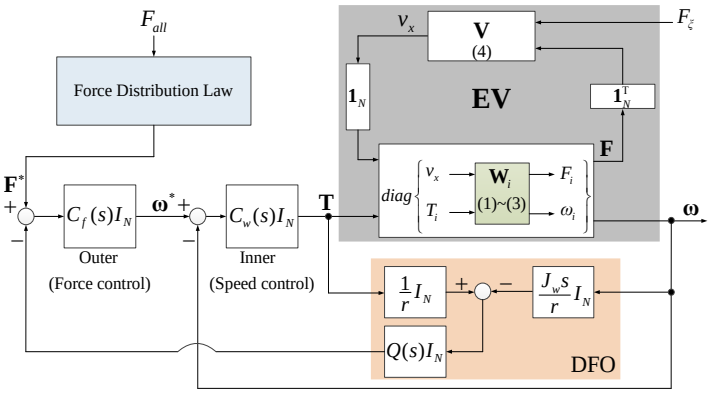

Fig. 3. Block diagram of the proposed driving force control system.

Notice 1: This paper focuses on the stability analysis of the driving force control system in Fig. 3. The algorithm to determine the maximum allowable wheel speed reference is not considered, as it is not the main goal of this paper.

IV. GLOCAL STABILITY ANALYSIS

The system in Fig. 3 can be seen as multi-agent system in which the local agent consists of the wheel dynamics $\mathbf{W}_i$, the force controller C_f, the speed controller C_w, and the local DFO. The local agents are diagonal, and they "interact" via the "aggregation" vector $\mathbf{1}_N^{\mathrm{T}}$, the vehicle dynamics $\boldsymbol{\mathcal{V}}$, and the "distribution" vector $\mathbf{1}_N$. Thus, it is possible to represent the system in Fig. 3 by the feedback connection of two parts. The first part is an interaction matrix, which is the multiplicity of the distribution and aggregation matrix. The second part is calculated based on $\mathbf{W}_i$, $\mathbf{V}$, C_f, C_w, and the DFO. Note that, only $\mathbf{W}_i$ contains the nonlinearities of the slip ratio definition (2) and the force model (3). Thus, a strategy to system analysis is to linearize (2) and (3). To this end, we examine the proposed DFC at an operating point $\mathbf{OP} = \{\omega_{o,1}, \ldots, \omega_{o,N}, v_{xo}\}$. The following assumptions are considered:

(i) The vehicle operates on the uniform road condition and the friction coefficients of four wheels are the same.

(ii) The slip ratio is small, and the driving force is linearized as $F_i = S_n\lambda_i$ where S_n is the nominal driving stiffness.

(iii) At the operating point, the values of $\max\{r\omega_{o,i}, v_{xo}, \varepsilon\}$ are almost the same. In other words, we might approximate:

$$\kappa_n \approx \frac{1}{\max\left\{r\omega_{o,i}, v_{xo}, \varepsilon\right\}} \quad \forall i \in [1, N]\,.$$

A. A linearized modelling of DFC system

With respect to the assumptions (i) ~ (iii), the driving force can be linearized as

$$F_i = S_{eqn}\eta_i \tag{7}$$

where $S_{eqn} = \kappa_n S_n$, and $\eta_i = r\omega_i - v_x$.

Neglecting the input disturbances, the system in Fig. 3 can be linearized as the system in Fig. 4(a) where $\mathrm{A} = \mathbf{1}_N\mathbf{1}_N^{\mathrm{T}}$ and:

$$G(s) = \frac{rC_f(s)P_w(s)}{rP_w(s) - C_f(s)Q(s)} \tag{8}$$

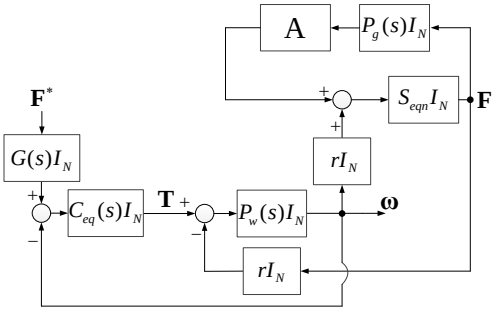

(a) Representation of the original DFC system by linearizing wheel dynamics.

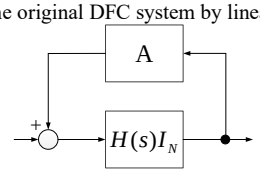

(b) Equivalent expression for glocal stability analysis.

Fig. 4. Linearized expression of the DFC system.

$$C_{eq}(s)=\frac{\left[rP_w(s)-C_f(s)Q(s)\right]C_w(s)}{P_w(s)\left[r+C_f(s)C_w(s)Q(s)\right]},\ P_w(s)=\frac{1}{J_w s},\ P_g(s)=\frac{1}{ms} \quad (9)$$

For the purpose of stability analysis, the Force Distribution Law, which only generates the reference forces, is not considered. The system in Fig. 4(a) can be represented as the system $\sum(H(s),\mathrm{A})$ in Fig. 4(b) with:

$$H(s)=\frac{S_{eqn}\left[1+C_{eq}(s)P_w(s)\right]P_g(s)}{1+C_{eq}(s)P_w(s)+S_{eqn}r^2P_w(s)} \quad (10)$$

Notice 2: $\sum(H(s),\mathrm{A})$ is a multi-agent system with the local dynamics $H(s)$ and the physical interaction matrix A of rank-1. In other words, matrix A has $N-1$ zero eigenvalues, and one non-zero eigenvalue which equals to $-N$.

B. Stability analysis

The system in Fig. 4(b) is stable at $\mathcal{O}$ if and only if

$$\rho_i H(s)-1\neq 0\ \ \forall s\in\mathbb{C}_+ \quad (11)$$

holds true for all eigenvalues ρ_i of matrix A. Following the generalized frequency variable (GFV) theory [13] with respect to **Notice 2**, the condition (11) is satisfied if the point $(-N,0)$ is located in the stable domain Ω_+^c defined as:

$$\Omega_+ \coloneqq \phi(\mathbf{C}_+),\ \Omega_+^c \coloneqq \mathbf{C}\setminus\Omega_+$$

where $\phi(s)=H^{-1}(s)$ is the GFV. However, the stable condition is not enough. To address the damping ratio and convergence rate rather than just guaranteeing the stability, it is essential to analyze the **D**-stability. One of typical **D**-stability region useful for the practical application of IWM-EV is illustrated in Fig. 5. Define the half-plane as

$$\mathbf{C}_{\alpha,\beta}\coloneqq\left\{s\in\mathbf{C}:\mathrm{Re}\left(e^{-j\beta}s+\alpha\right)<0\right\} \quad (12)$$

As depicted in Fig. 5, region **D** is constructed by the intersection of four half-planes. In other words, we have:

$$\mathbf{D}=\mathbf{C}_{0,\theta}\cap\mathbf{C}_{0,-\theta}\cap\mathbf{C}_{\alpha_1,0}\cap\mathbf{C}_{\alpha_2,0}$$

where $0<\theta<\pi/2$ and $0<|\alpha_1|<|\alpha_2|$. We notice that $\mathbf{C}_{\alpha,\beta}$ is derived by rotating $\mathbf{C}_-$ by an angle $-\beta$ counterclockwise

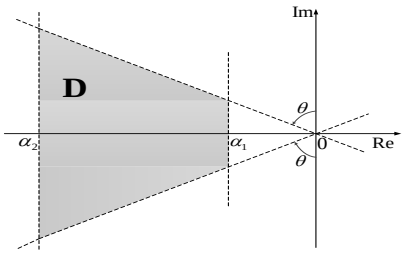

Fig. 5. Definition of region **D**.

around the origin and shifting the resulting region by α in the direction of the real axis. Therefore, all the poles of $\sum(H(s),\mathrm{A})$ belong to $\mathbf{C}_{\alpha,\beta}$ if all the eigenvalues of matrix A are located in the domain $\Lambda^{\mathbf{C}}(\alpha,\beta)$ which is established by applying the extended Routh-Hurwitz criterion to the GFV in which "s" is transformed into "$e^{-j\beta}s+\alpha$". An algorithm to derive $\Lambda^{\mathbf{C}}(\alpha,\beta)$ can be referred to the Appendix A, B, and C of Ref. [13]. The **D**-stability condition is stated as follows.

D-stability condition: The DFC system is **D**-stable at an operating point **OP** if $H(s)$ is **D**-stable and two points $(-N,0)$ and $(0,0)$ are located in the domain defined as

$$\Lambda=\Lambda^{\mathbf{C}}(0,\theta)\cap\Lambda^{\mathbf{C}}(0,-\theta)\cap\Lambda^{\mathbf{C}}(\alpha_1,0)\cap\Lambda^{\mathbf{C}}(\alpha_2,0).$$

V. DEMONSTRATION OF THE PROPOSED STRATEGY

This paper utilizes the 4-wheel EV shown in Fig. 1(a). The main parameters of the vehicle are summarized in Table 1. As an example, we will design the force and speed controllers of the proportional integral (PI) type:

$$C_f(s)=\frac{K_{Pf}s+K_{If}}{s},\ C_w(s)=\frac{K_{Pw}s+K_{Iw}}{s} \quad (13)$$

A. System design and analysis

Substituting (13) into (10), we have:

$$\phi(s)=\frac{1}{H(s)}=\frac{s^4+a_3s^3+a_2s^2+a_1s+a_0}{b_3s^3+b_2s^2+b_1s+b_0} \quad (14)$$

where

$$b_3=S_{eqn}m^{-1},b_2=S_{eqn}\left(K_{Pw}\tau+J_w\right)\left(mJ_w\tau\right)^{-1}$$

$$b_1=S_{eqn}\left(K_{Iw}\tau+K_{Pw}\right)\left(mJ_w\tau\right)^{-1},b_0=S_{eqn}K_{Iw}\left(mJ_w\tau\right)^{-1}$$

$$a_3=\left(K_{Pw}\tau+J_w+r^3S_{eqn}\tau\right)\left(J_w\tau\right)^{-1}$$

$$a_2=\left(K_{Iw}\tau+K_{Pw}+r^2S_{eqn}\tau+r^2S_{eqn}K_{Pf}K_{Pw}\right)\left(J_w\tau\right)^{-1}$$

$$a_1=\left(K_{Iw}+r^2S_{eqn}K_{If}K_{Pw}+r^2S_{eqn}K_{Pf}K_{Iw}\right)\left(J_w\tau\right)^{-1}$$

$$a_0=r^2S_{eqn}K_{If}K_{Iw}\left(J_w\tau\right)^{-1}$$

Following Theorem 1 in [13], the domain Ω_+^c is obtained by firstly defining the polynomial:

$$\phi(s)=\frac{1}{H(s)}=\frac{s^4+a_3s^3+a_2s^2+a_1s+a_0}{b_3s^3+b_2s^2+b_1s+b_0} \quad (15)$$

Table 1. Specifications of the experimental vehicle.

Symbol	Description	Value
m	Vehicle mass	925 kg
J_w	Wheel radius	0.302 m
r	Wheel moment of inertia	1.26 kg.m^2
–	Front motor's maximum torque	500 N.m
	Front motor's maximum power	20.0 kW
–	Rear motor's maximum torque	340 N.m
–	Rear motor's maximum power	10.7 kW

Then, Ω_+^c is obtained by a set of inequality $\{D_k > 0\}$ which is calculated as

$$\begin{cases} D_1 = \det|p_1| \\ D_k = \det\begin{bmatrix} F(\mathbf{p}_k) & -F(\mathbf{q}_k)R \\ UF(\mathbf{q}_k) & F(\mathbf{p}_{k-1}) \end{bmatrix} \quad (k = 2,\ldots,4) \end{cases} \tag{16}$$

where the vectors $\mathbf{p}_k$, $\mathbf{q}_k$, and the matrices R, U, F can be found in [13]. Notice that in the procedure (16): $p_i = q_i = 0$ if $i > 4$.

Considering the 4-in-wheel-motor EV, we have $N = 4$ and matrix A has one non-zero eigenvalue which is placed at $(-4, 0)$. The region **D** is specified by a set of parameters $\theta = 2\pi/3$, $\alpha_1 = 2$, and $\alpha_2 = 30$. By a fine-tuning process with pole-placement to the closed-loop system including $P_w(s)$ and $C_w(s)$, the speed controller is selected with $K_{Pw} = 50.48$ and $K_{Iw} = 504.76$. The time constant of the DFO's low-pass filter is chosen as $\tau = 0.03$ $[s]$. The force control gains are selected as $K_{Pf} = 0.02$ and $K_{If} = 2.00$.

This paper examines the operating point with v_{xo} = 5 [m/s], and the vehicle runs on a high friction surface with the nominal friction coefficient μ = 0.8. It is assumed that a small slip ratio of 0.05 is maintained constantly when the vehicle velocity changes between $v_{xo} - \Delta v$ and $v_{xo} + \Delta v$ where Δv = 2 [m/s]. Applying the **D**-stability condition in the previous Section, the stable regions given by the GFV at v_{xo}, $v_{xo} - \Delta v$ and $v_{xo} + \Delta v$ are plotted as the shaded regions in Figs. 6(a), (b), and (c), respectively. Transparently, the system has enough stability margin and the points $(-4, 0)$ and $(0, 0)$ are always placed in such shaded regions. This shows that the above controller design guarantees the **D**-stability of the DFC system.

B. Experimental evaluation of driving force control

To evaluate the tracking performance of the proposed DFC, experiment was conducted at our test course in Kashiwa Campus, the University of Tokyo. The vehicle was accelerated with a driving force command equally distributed to each wheel. The experimental results of the vehicle speed and wheel speed are shown in Fig. 7(a). The driving force reference of 700 [N] and the actual driving force are shown in Fig. 7(b). For the sake of clearness, we only described the data of the rear left wheel. Test results confirm that the vehicle was smoothly accelerated and the actual driving forces successfully follow the reference value.

For comparison, driving force control using a simple feedforward strategy was also performed. This means the motor torque was directly generated from the reference as $T_i = r \times F_i^*$. As shown in Fig. 7(c), the feedforward force control suffers a large tracking error. Thus, it is necessary to utilize feedback force control strategy for the goal of accurate force distribution.

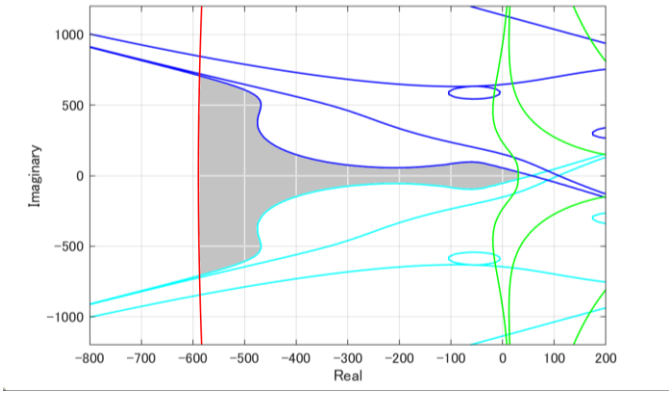

(a) Stable domain plotted at v_{xo}.

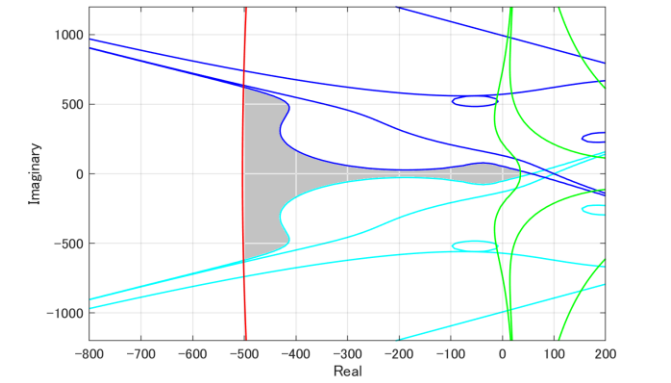

(b) Stable domain plotted at $v_{xo} - \Delta v$.

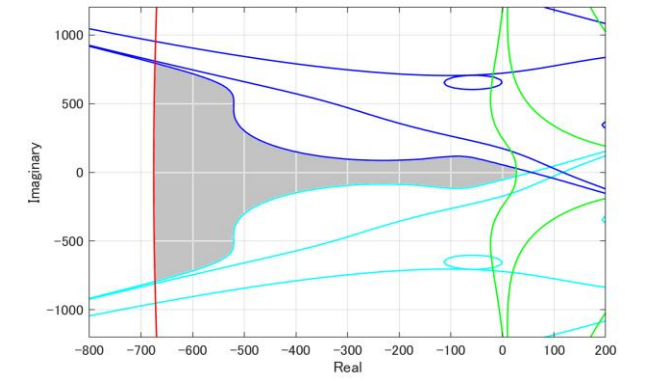

(c) Stable domain plotted at $v_{xo} + \Delta v$.

Fig. 6. **D**-stability at different operating points.

C. Application to range extension control

Our research group has developed the range extension control system (RECS) for optimizing the use of electric energy [15], [16]. To this end, the motor torques are distributed by minimizing the total of motor input power. However, the previous studies did not examine the accurate force allocation. This paper extends the original idea of RECS by utilizing the proposed DFC.

The *i*th motor output power is $P_{out,i} = \omega_i T_i$. From (2), the motor speed can be approximated as $\omega_i \approx v_x(1 + \lambda_i)/r$. As discussed in the previous Section, the driving force is linearized

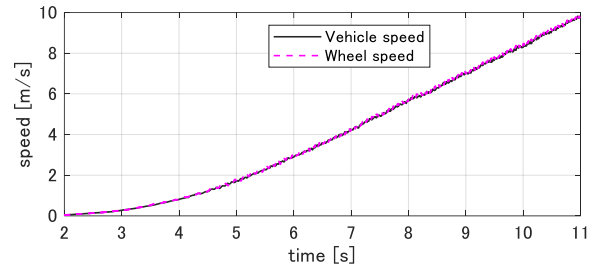

(a) Vehicle speed and wheel speed.

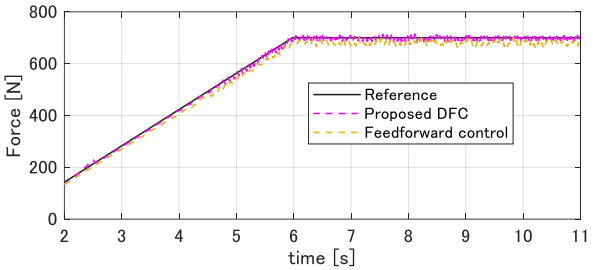

(b) Driving force.

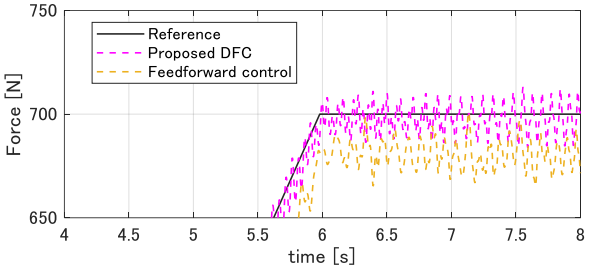

(c) Comparison of force tracking error.

Fig. 7. Experimental results of wheel speed based DFC.

as $F_i = S_n \lambda_i$. From the vehicle dynamics equations (1) ~ (4), the relationship between the motor torque and the driving force can be approximated as $T_i \approx r_{eq} F_i$ where $r_{eq} = r + NJ_w/(rm)$. Let k_i be the force distribution ratio ($k_1 + \cdots + k_N = 1, 0 < k_i < 1$), the motor output power is approximately expressed as

$$P_{out,i} = \frac{v_x}{r}\left(1 + \frac{k_i F_{all}}{D_{s,i}}\right) r_{eq} k_i F_{all} \tag{17}$$

The EV in Fig. 1(a) is driven by permanent magnet synchronous motor (PMSM). Using the motor parameters summarized in [15], it is reasonable to assume that the d-axis currents are maintained small. Based on the equivalent circuit of the PMSM [17], the copper-loss and iron-loss powers are derived as follows:

$$P_{cu,i} = R_{a,i}\left[\left(\frac{v_x \rho_i L_{d,i}}{r R_{c,i}} \frac{k_i r_{eq} F_{all}}{\Psi_{a,i}}\right)^2 + \left(\frac{k_i r_{eq} F_{all}}{p_{n,i} \Psi_{a,i}} + \frac{p_{n,i} v_x \Psi_{a,i}}{r R_{c,i}}\right)^2\right] \tag{18}$$

$$P_{fe,i} = \frac{p_{n,i}^2}{r^2 R_{c,i}}\left(\Psi_{a,i}^2 + \frac{\rho_i^2 L_{d,i}^2 k_i^2 r_{eq}^2 F_{all}^2}{p_{n,i}^2 \Psi_{a,i}^2}\right) \tag{19}$$

where the armature winding resistance and the iron loss resistance are $R_{a,i}$ and $R_{c,i}$, respectively. $L_{d,i}$ and $L_{q,i}$ are the d- and q-axis components of the armature self-inductance, respectively. The number of poles pairs is $p_{n,i}$, and the motor salient coefficient is $\rho_i = L_{q,i}/L_{d,i}$. Let $\Psi_{e,i}$ be the flux linkage of the permanent magnet per phase, we have $\Psi_{e,i} = \sqrt{3}\Psi_{e,i}$.

In summary, the optimization problem of the Force Distribution Law is expressed as:

$$\min_{\{k_i\}} \sum_{i=1}^{N}\left(P_{out,i} + P_{cu,i} + P_{fe,i}\right) \quad \text{s.t.} \sum_{i=1}^{N} k_i = 1, 0 < k_i < 1 \tag{20}$$

From (17) ~ (19), the cost function in (20) is shown to be a quadratic function of k_i. Thus, giving the total driving force command F_{all} and the vehicle speed v_x the optimal distribution gains can be obtained in real-time without special difficulty.

The setting of the range extension control test is shown in Fig. 8 where Fig. 8(a) describes the speed pattern, and Fig. 8(b) describes the change of road friction coefficient in the longitudinal direction. Three test cases were performed for comparison.

- **Case 1**: The vehicle is controlled by the proposed DFC system. However, the driving force distribution ratios are fixed at some values. For instance, the distribution ratios of the front and rear wheels are $0.5(1-q)$ and $0.5q$, respectively. The value q is selected as a number in the set $\{0.0, 0.1, 0.2, \ldots\ 0.9, 1.0\}$.
- **Case 2**: The RECS [15] is utilized. This method can be seen as a feedforward driving force control. The motor torque is distributed to minimize the total of motor input power.
- **Case 3**: The proposed DFC system is utilized with the force distribution law (20). Note that, the local DFC of each wheel is provided with a wheel speed limiter, which was presented in our recent work [10].

The energy consumptions of the vehicle in the above test cases are summarized in Fig. 9. By varying the force distribution ratio, the energy consumption of Case 3 is smaller than Case 1 for any fixed ratios q. On the other hand, the feedforward force

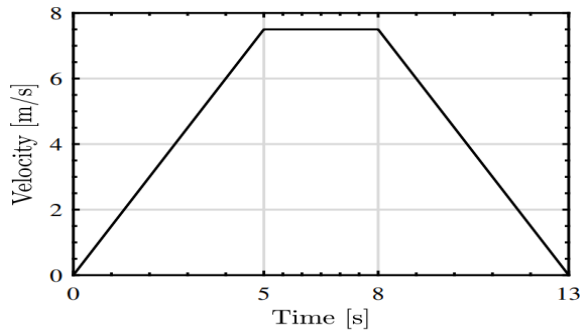

(a) Vehicle speed pattern.

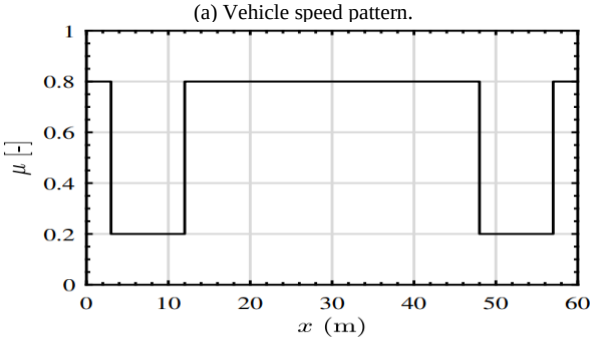

(b) Map of road friction coefficient.

Fig. 8. Setup of range extension control test.

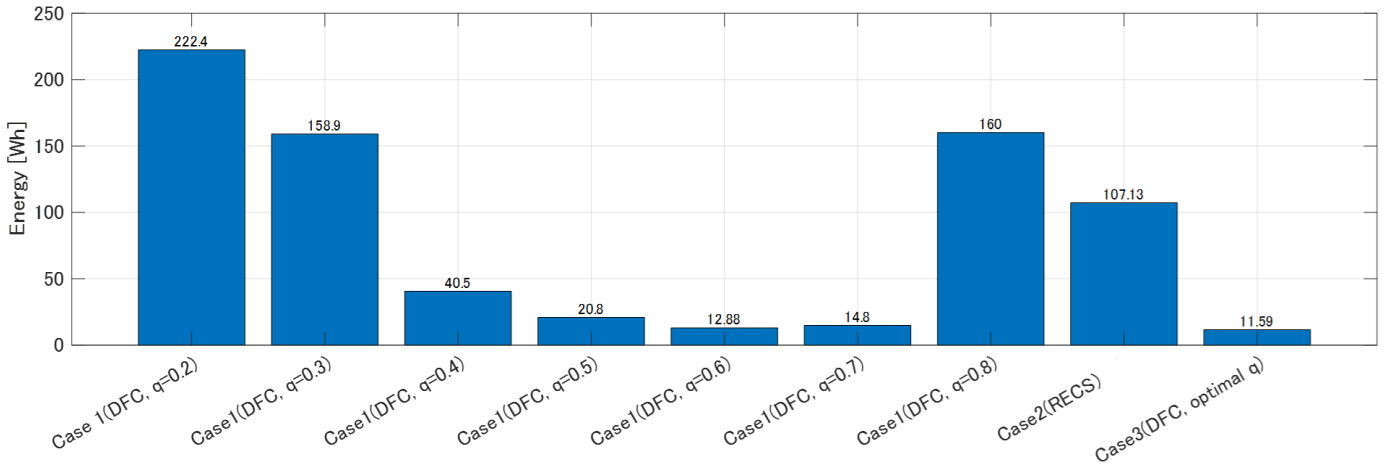

Fig. 9. Energy consumption with different strategies [Wh].

control based RECS in Case 2 cannot prevent the wheel slip due to the change of road friction coefficient. Although Case 2 distributes the motor torques by minimizing motor input power, its energy consumption is much bigger than Case 3, and Case 1 with the selection of $q = \{0.4, 0.5, 0.6, 0.7\}$.

VI. Conclusions

Based on GFV theory, this aper generalizes the wheel speed based DFC, and improves the stability condition which was presented in [10]. It clarifies that IWM-EVs should be treated as multi-agent systems with rank-1 physical interaction. The modelling of this paper, therefore, can be utilized to design other motion control systems for multi-motor vehicles, including the mecanum-wheel-robots in Fig. 1. In future study, the **D**-stability test can be improved to address the variation of the driving stiffness and the uncertainties of physical parameters, such as vehicle mass and wheel inertia. The proposed DFC is shown to be a promising framework for energy optimization of electric vehicle. Experiments of the proposed method under road condition change will be performed for further discussion and evaluation.

Acknowledgement

This work is partly supported by the Nagamori Research Grants for young researcher.

References

[1] B.-M. Nguyen, J. P. F. Trovao, M. C. Ta and M. Kawanishi, “Longitudinal Motion Control of Electric Vehicles: Glocal Model and Design Using Passivity,” IEEE Vehicular Technology Magazine, Vol. 16, No. 3, pp. 75-86, 2021.

[2] L. Cai, Z. Liao, S. Wei and J. Li, “Novel Direct Yaw Moment Control of Multi-Wheel Hub Motor Driven Vehicles for Improving Mobility and Stability,” IEEE Transactions on Industry Applications, Vol. 59, No. 1, pp. 591-600, 2023.

[3] P. Stano *et al*., “Enhanced Active Safety Through Integrated Autonomous Drifting and Direct Yaw Moment Control via Nonlinear Model Predictive Control,” IEEE Transactions on Intelligent Vehicles, vol. 9, no. 2, pp. 4172-4190, 2024.

[4] Y. Ikezawa, H. Fujimoto, D. Kawano, Y. Goto, Y. Takeda and K. Sato, “Range Extension Autonomous Driving for Electric Vehicle Based on Optimal Vehicle Velocity Profile in Consideration of Cornering,” Electrical Engineering in Japan, Vol. 207, Iss. 1, pp. 43-54, 2019.

[5] K. Kwon, D. -M. Kim, K. -S. Cha, J. Jo, M. -S. Lim and S. Min, "Multi-objective optimization of two-motor and two-speed system for electric vehicles considering motor characteristics," IEEE Transactions on Transportation Electrification, 2024 (Early Access).

[6] T. Suzuki, M. Mae, T. Takeuchi, H. Fujimoto, and E. Katsuyama, “Model-based Filter Design for Triple Skyhook Control of In-wheel Motor Vehicles for Ride Comfort,” IEEJ Journal of Industry Applications, Vol. 10, Iss. 3, pp. 310-316, 2021.

[7] M. Yoshimura and H. Fujimoto, “Driving Torque Control Method for Electric Vehicle with In-wheel motors,” Electrical Engineering in Japan, Vol. 181, No. 3, pp. 49–58, 2012.

[8] K. Maeda, H. Fujimoto, and Y. Hori, “Four-wheel Driving-force Distribution Method for Instantaneous or Split Slippery Roads for Electric Vehicle,” Automatika, Vol. 54, No. 1, pp. 103-113, 2013.

[9] H. Fuse and H. Fujimoto, “Fundamental Study on Driving Force Control Method for Independent-Four-Wheel-Drive Electric Vehicle Considering Tire Slip Angle,” 44th Annual Conference of the IEEE Industrial Electronics Society, pp. 2062-2067, 2018.

[10] T. Ueno, B. -M. Nguyen and H. Fujimoto, “Driving Force Control for In-Wheel Motor Electric Vehicles with Wheel Speed Limiter and Absolute Stability Analysis,” 49th Annual Conference of the IEEE Industrial Electronics Society, pp. 1-6, 2023.

[11] T. Ueno, B.-M. Nguyen, and H. Fujimoto, “Direct yaw moment control for electric vehicles with variable-rate-slip-ratio-limiter based driving force control,” IEEE International Conference on Mechatronics, pp. 1-6, 2023.

[12] B-M. Nguyen, S. Hara, H. Fujimoto, and Y. Hori, “Slip Control for IWM Vehicles Based on Hierarchical LQR,” Control Engineering Practice, Vol. 93, 104179, 2019.

[13] S. Hara, H. Tanaka, and T. Iwasaki, “Stability Analysis of Systems with Generalized Frequency Variables,” IEEE Transactions on Automatic Control, Vol. 59, No. 2, pp. 313-326, 2014.

[14] H. B. Pacejka, “Tyre and Vehicle Dynamics,” Third Edition, Published by SAE International and Butterworth Heinemann with a Product Code of R-418, ISBN of 978-0-0809-7016-5, 2012.

[15] H. Fujimoto and S. Harada, “Model-Based Range Extension Control System for Electric Vehicles with Front and Rear Driving–Braking Force Distributions,” IEEE Transactions on Industrial Electronics, Vol. 62, No. 5, pp. 3245-3254, 2015.

[16] B. -M. Nguyen, J. P. F. Trovão and M. C. Ta, “Double-Layer Energy Management for Multi-Motor Electric Vehicles,” IEEE Transactions on Vehicular Technology, Vol. 72, No. 7, pp. 8623-8635, 2023.

[17] S. Morimoto, Y. Tong, Y. Takeda and T. Hirasa, “Loss Minimization Control of Permanent Magnet Synchronous Motor Drives,” IEEE Transactions on Industrial Electronics, Vol. 41, No. 5, pp. 511-517, 1994.